Available online at www.sciencedirect.com
ScienceDirect
Acta Materialia 59 (2011) 159–170
Acta MATERIALIA
www.elsevier.com/locate/actamat

# Networked interpenetrating connections of icosahedra: Effects on shear transformations in metallic glass

Mirim Lee [a], Chang-Myeon Lee [a,b], Kwang-Ryeol Lee [c], Evan Ma [d], Jae-Chul Lee [a,*]

[a] Department of Materials Science and Engineering, Korea University, Seoul 136-701, Republic of Korea
[b] Nano-surface Technology Center, Korea Institute of Industrial Technology, Incheon 404-254, Republic of Korea
[c] Computational Science Center, Korea Institute of Science and Technology, Seoul 136–791, Republic of Korea
[d] Department of Materials Science and Engineering, Johns Hopkins University, Baltimore, MD 21218, USA

Received 5 January 2010; received in revised form 9 September 2010; accepted 10 September 2010
Available online 11 October 2010

**Abstract**

The local structures of metallic glasses have been analyzed previously in term of various types of short-range order (SRO). However, the SRO alone, neglecting the interconnection of neighboring icosahedra to medium range and beyond, is insufficient to account for the structure–property relationship in metallic glasses. In this study, we use molecular dynamics (MD) simulations of Cu–Zr binary metallic glasses to examine the effects of the next level of structural hierarchy: the interpenetrating connection of icosahedra (ICOI) and the linkage of the medium-range ICOI patches to form networks of icosahedra over extended range. The mechanical properties of these metallic glasses, especially the shear transformations that mediate plasticity, are found to be dependent on the degree of ICOI and development of the ICOI network. The evolution of the ICOI network during shear deformation, as well as the composition dependence, has been monitored and discussed.


*Keywords:* Amorphous alloy; Metallic glass; Short-(medium-)range order; Plasticity; Molecular dynamics

## 1. Introduction

The mechanical properties, especially plasticity, of metallic glasses depend largely on their atomic-scale structures, to an extent similar to that of crystalline materials. However, the details of the atomic-scale structures of the metallic glasses, and especially those that are responsible for their properties, remain to be elucidated. In 1928, Ramsey [1] proved that every complex structure, while seemingly random, necessarily contains ordered substructures. Nevertheless, it was not until much later that researchers began to recognize the existence of short-range-ordered structures (SROs) in metallic glasses, and relate these fundamental structural motifs to macroscopic properties. In recent years, Miracle [2], Sheng et al. [3] and Yang et al. [4] described the local structures of the amorphous solid based on quasi-equivalent clusters of various fractions, while Shi and Falk [5] related the SRO structure, and different degree of SROs obtained by changing the cooling rate, to the strain localization in the metallic glasses. Subsequently, Wakeda et al. [6], Lee et al. [7], Park et al. [8], and Cheng et al. [9] performed extensive studies to clarify the composition dependency of the SRO structures in Cu–Zr-based metallic glasses and to relate these SROs to the observed mechanical properties. Shi and Falk [5,10] also assessed the effects of another important structural parameter, i.e., the spatial distribution and percolation of SRO, on the mechanical response. However, for this latter issue, much remains to be uncovered and analyzed in detail, as discussed below.

Recent atomic simulations revealed that the local structure of metallic glasses can comprise more than 100 different types of polyhedra. These local motifs, representing different SROs, are the building blocks of the three-dimen-

* Corresponding author. Tel.: +82 2 3290 3283; fax: +82 2 928 3584.
*E-mail address:* jclee001@korea.ac.kr (J.-C. Lee).

1359-6454/$36.00 © 2010 Acta Materialia Inc. Published by Elsevier Ltd. All rights reserved.
doi:10.1016/j.actamat.2010.09.020

sional glassy structure. Intuitively, even with the same fractions of the various SROs, innumerable numbers of different structures can be made by simply rearranging these SROs, which in turn can produce different mechanical properties. As such, the structure–property relation cannot be established by considering the SROs alone. It is therefore necessary to consider the glassy structure in a hierarchical sense. From this perspective, naturally the next task is to examine the structural organization beyond SROs (the first level clusters), to probe into the next level of the structural hierarchy. In other words, it is of importance to uncover the various ways the SROs are connected with one another and how the type and degree of connections affect the mechanical response of the amorphous material. This will be attempted in this paper, and can be viewed as a stepping stone before probing into an even higher hierarchical level, i.e., the percolation of structural order throughout the entire sample, to quantitatively establish if the amorphous solid has a backbone and how that influences the properties [11].

SROs generated during cooling tend to fill the 3D space of the metallic glasses in an efficient way to attain the lowest possible energy state under the kinetic constraints. As will be discussed later, this can be achieved by forming a densely packed structure, in which SROs connect with neighboring SROs to construct the medium-range-ordered structures (MROs). These MROs are atomic-scale structures with length scales typically longer than the diameter of the third coordination shell but shorter than the scale at which ordering becomes long-range and Bragg peaks appear in the structure factor [12]. It has been difficult to observe the MROs experimentally using conventional electron microscopy and diffractometry. Recently, the existence of MROs within disordered materials was suggested in fluctuation electron microscopy experiments [13,14]. Some specific types of MROs in metallic glasses were proposed from the model studies on efficient packing [15,16]. Several configurations of MROs have also been identified via the combined use of experiments (such as X-ray scattering) and atomistic simulations [16–22]. However, many other types of medium-range structures are possible, beyond the examples of MROs reported in earlier studies. Further, it has not been established whether the reported MROs are the major structural organization that plays a key role in determining the mechanical properties.

In this study, using molecular dynamics (MD) simulations of Cu–Zr binary alloys, we illustrate a conceptual structural organization, i.e., interpenetrating connection of icosahedra (ICOI) over an extended range. The characteristics of the networked structure based on ICOIs are quantitatively assessed in terms of their connectivity and rigidity. We also explore how the ICOI networks are created during cooling and destroyed during shear deformation, in order to qualitatively relate their evolution behaviors to the mechanical properties of metallic glasses, in the context of the nucleation of local shear deformation and the strain localization.

## 2. Molecular dynamics (MD) simulations and structural analysis

Atomic simulations, due to their ability to depict the atomic-scale structures and the corresponding mechanical properties, have been a powerful technique to explore the structure–property relationship in metallic glasses [2,5,6,9–11]. Of the various simulation techniques presently available, the first-principles calculations provide the most reliable interatomic interactions. However, these calculations are based on the NVT (constant numbers of atoms, volume and temperature) ensemble, which is different from the real-world laboratory conditions. In addition, the typical size that can be handled by this method is too small (normally less than ~200 atoms), and thus produces significant statistical scatter and is inadequate to investigate the mechanical behaviors of materials. Another approach is to use classical MD simulations employing (semi-)empirical interatomic potentials that can manage millions of atoms and the NPT (constant numbers of atoms, pressure and temperature) ensemble. Although MD simulations suffer from severe spatial and temporal limitations and their accuracy relies critically on the potential, this technique has been widely used to explore the structure–property relation by describing the general features of the local structure and its evolution associated with shear deformation [7–9,11], which cannot feasibly be obtained experimentally.

To investigate the structural changes and associated deformation behaviors of metallic glasses, we selected two model alloys from the Cu–Zr binary system: $Cu_{50}Zr_{50}$ and $Cu_{65}Zr_{35}$. These alloys possess a pronounced difference in their initial packing densities (or atomic-scale packing structures) and thus exhibit clearly different structural evolutions and associated flow behaviors [7,8]. These alloy characteristics enabled the investigation to focus on the effects exerted by the atomic packing structures of these alloys on both the structural evolution and the corresponding mechanical responses.

The 3D binary alloys were constructed using MD simulations employing the embedded atom method (EAM) potential developed by Cheng et al. [9,23]. Approximately 32,000 atoms corresponding to the $Cu_{50}Zr_{50}$ and $Cu_{65}Zr_{35}$ compositions were first packed into the simulation cell with approximate dimensions of $7.9 \times 10.1 \times 6.4$ nm and then heated to 2000 K. After allowing a sufficient relaxation time of 1 ns (time step 1 fs), the alloys were cooled to 300 K at a rate of $5 \times 10^{12}$ K s$^{-1}$ to produce the 3D amorphous solids. The NPT ensemble was used for quenching, with the temperature controlled by a Nose–Hoover thermostat [24] and the pressure controlled at zero using a Nose–Hoover barostat [25]. A periodic boundary condition (PBC) was applied to the 3D directions in order to eliminate surface effects.

The model alloys with PBC were deformed at 300 K by applying simple shear with a strain rate of $10^8$ s$^{-1}$ to induce plastic deformation and structural disordering. The

atomic-scale structures of the quenched alloy and their evolution during simple shear deformation were analyzed in terms of SROs identified using the weighted-Voronoi tessellation technique (hereafter, Voronoi analysis) [26]. Further analyses were conducted to examine the connections of neighboring SROs to construct MROs.

## 3. 3D atomic configuration and SROs

The two metallic glasses, $Cu_{50}Zr_{50}$ and $Cu_{65}Zr_{35}$, were first synthesized using MD to dimensions smaller than the typical thickness (~10–20 nm) of shear bands. As such, the entire box will undergo homogeneous deformation upon applying a shear load. As known from previously reported experimental and simulation studies on the structure–property relations [7–9,27,28], these two metallic glasses have clearly different structures and mechanical properties.

Fig. 1a shows an example of the typical 3D atomic configuration of the amorphous $Cu_{65}Zr_{35}$. Although the potential used for MD simulations has already been extensively validated against a large set of experimental properties and ab initio data [29], the reliability of the potential was tested again by comparing the average interatomic distances of the nearest atomic pairs comprising the model alloys with the experimental measurements. The nearest average interatomic distances of the Cu–Cu, Cu–Zr and Zr–Zr pairs were determined by calculating the partial radial distribution functions (RDFs) of $Cu_{65}Zr_{35}$, as shown in Fig. 1b. Calculations of the partial RDFs were also conducted for $Cu_{50}Zr_{50}$. The present calculations agreed reasonably well with the experimental measurements obtained using high-energy X-ray diffractometry [30–33,36] and simulations from other reported empirical potentials [34–37]. This lends support to the ability of the EAM potential used in this study to describe the local structures of the actual metallic glasses.

The local structures of the model alloys were analyzed in terms of the various SROs identified using the Voronoi tessellation technique. Among the various SROs, the icosahedron, denoted by the Voronoi index (0,0,12,0), possesses a high atomic packing density (equivalently low free volume) and five-fold nearest-neighbor bonds, and is known to be mechanically and energetically more stable than other types of SROs [9,39]. In the following, the spatial distributions of icosahedra and their linking patterns will be shown to also play an important role in determining the local deformation behaviors and thus the overall mechanical properties of the sample.

## 4. Icosahedra and icosahedral MROs

Although the five-fold icosahedra are unable to build a structure with a long-range order, in an amorphous alloy, they can link together to form extended clusters (of icosahedra) [29]; the length scales of these icosahedra patches are typically beyond the diameter of the third coordination shell and often extend to nanometer range. According to the Voronoi analysis shown in Fig. 2a, the majority (85–98%, depending on composition) of icosahedra in $Cu_{50}Zr_{50}$ and $Cu_{65}Zr_{35}$ exist in the form of linked clusters, rather than isolated ones. These extended clusters of icosahedra are made of icosahedra that interconnect to neighbor icosa-

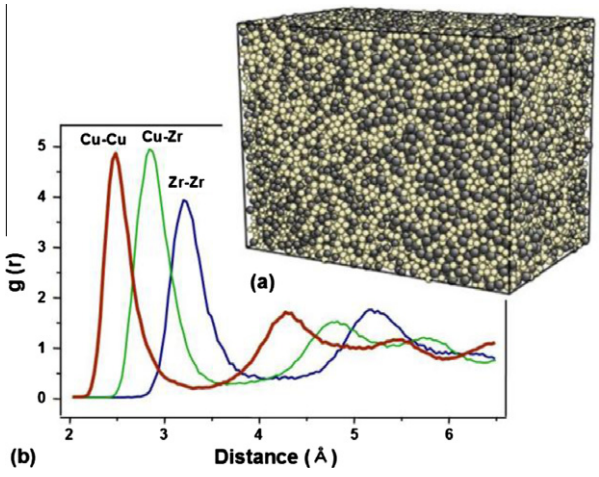


Fig. 1. (a) Typical 3D atomic configuration of the computational $Cu_{65}Zr_{35}$ amorphous alloy constructed using MD simulations employing the EAM potential. The yellow (small) and grey (large) spheres indicate Cu and Zr atoms, respectively. (b) Partial RDFs computed for Cu–Cu, Cu–Zr and Zr–Zr pairs. (For interpretation of the references to colour in this figure legend, the reader is referred to the web version of this article.)

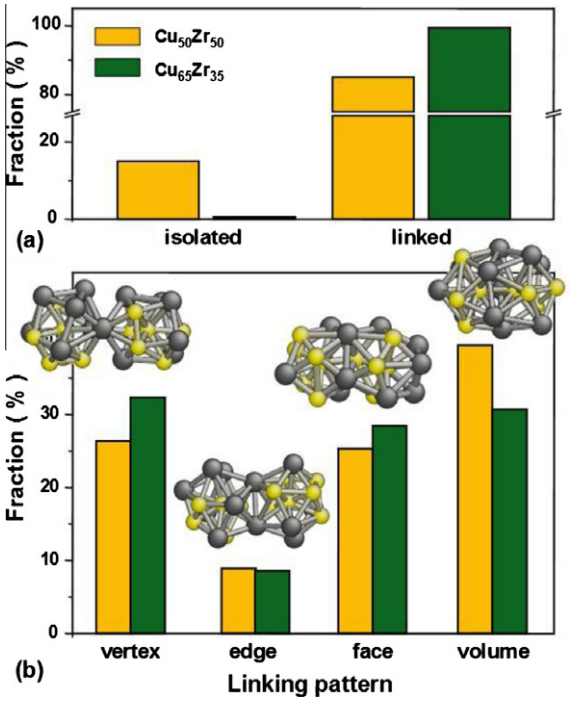


Fig. 2. (a) Fractions of the isolated and linked icosahedra, and (b) fractions of four different categories of MROs formed by sharing the vertex, edge, face and volume with neighboring icosahedra. The figures in the inset are the representative configurations for the different sharing type.

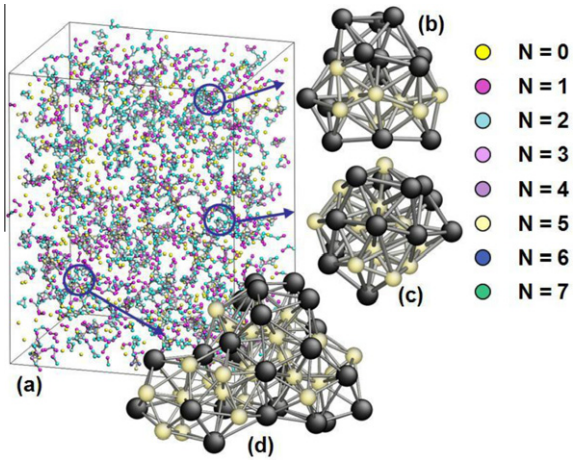


Fig. 3. (a) Representative snapshot showing the spatial distribution of the icosahedra comprising the $Cu_{65}Zr_{35}$ amorphous solid. Typical configurations of ICOIs with different bond numbers of (b) $N = 2$, (c) $N = 3$, and (d) $N = 6$. The yellow (small) and grey (large) spheres indicate Cu and Zr atoms, respectively. (For interpretation of the references to colour in this figure legend, the reader is referred to the web version of this article.)

hedral clusters by sharing their vertex, edge, face or volume, thereby forming four different types of connections [38], as shown by the representative configurations in the inset of Fig. 2b. Despite the differences in the potentials employed in the simulations, the general tendency observed from this study was consistent regardless of the potentials including FS-EAM, [1] modified EAM[1] and Lennard-Jones [38] potentials (data not shown).

Of the four different icosahedral linking patterns in Fig. 2b, the volume-sharing pattern is of special interest. Hereafter, the MROs resulting from this particular type of linkage of the icosahedra are referred to as the "interpenetrating connection of icosahedra (ICOI)". In literature, this connection is also termed "pentagonal bicap-sharing" or "cap-sharing", depending on authors. This linking pattern is produced when some or all of the surrounding (shell) atoms of the center atom of an icosahedron are also centers of the neighboring icosahedra, constituting "interpenetrating" icosahedra by sharing "five" common neighbor atoms, as shown in the inset of Fig. 2b. Note that different linking patterns can lead to different structural stability. In this study, the structural stability of various different linking patterns of icosahedra was first evaluated by calculating the potential energy of the center atom of the individual icosahedra participating in the connection scheme. The average potential energy ($\overline{E}$) of icosahedra as evaluated by their center atoms varied depending on how these icosahedra are linked with neighboring ones. Of the linking patterns considered in this study, ICOI gives the lowest average potential energy (see Table 1) and smaller average atomic volume [39], which makes the interpenetrating clusters of icosahedra not only

[1] Simulations were conducted by the authors using the FS-EAM and modified EAM potentials shown in Refs. [60,33], respectively.

Table 1
Average potential energy ($\overline{E}$) calculated for the center atoms (Cu) of the icosahedron (with the common composition of $Cu_6Zr_7$) that connect to a neighboring icosahedron by sharing their vertex, edge, face or volume in $Cu_{65}Zr_{35}$ (here "sampling number" means the number of sampled clusters).

| Linking pattern | $\overline{E} \pm \sigma$ (eV) | Sampling no. |
|---|---|---|
| Vertex | $-3.4868 \pm 0.0441$ | 901 |
| Edge | $-3.4890 \pm 0.0444$ | 115 |
| Face | $-3.4898 \pm 0.0445$ | 878 |
| Volume | $-3.4903 \pm 0.0437$ | 927 |

energetically more favorable, but also structurally more stable (see Fig. 7b of Ref. [39]) than other types of connected icosahedral clusters. By this argument, of the various MROs, the ICOI is likely to be the most important type of MRO affecting the mechanical properties of metallic glasses, as will be demonstrated later.

After deciding on the important icosahedral sharing scheme (the interpenetrating type, ICOI), the next characteristic to examine is how well and extensive the ICOI is, i.e., how many icosahedra neighbors an icosahedron is connecting with, in this particular volume-sharing way. Fig. 3a is an example showing the spatial distributions of icosahedra comprising $Cu_{65}Zr_{35}$. After assessing the structures of the model alloy using Voronoi analysis, only the atoms centered at the icosahedra are indicated as the points in the simulation cell. The points are colored to indicate how individual icosahedra are linked with neighboring icosahedra to form ICOI. This allows the observation that each icosahedron participates in the formation of ICOIs to various degrees by sharing its volume with different numbers of neighboring icosahedra; this number (i.e., how many neighbors in the first-coordination shell are also centers of other icosahedra) is referred to hereafter as the bond number, $N$, which quantifies the degree of ICOI. A high $N$ for an icosahedron means that this icosahedron bonds with (i.e., is forming ICOI with) many other icosahedra via volume sharing. $N$ is observed to range from 0 to 8. Some representative configurations of ICOIs with different bond numbers are shown in Fig. 3b–d.

Fig. 4a shows the population of icosahedra with various $N$. The population of non-interpenetrating icosahedra ($N = 0$) and ICOIs ($N \geqslant 1$) in the alloy differs depending on composition, and is higher in the alloy with a higher packing density, i.e., $Cu_{65}Zr_{35}$. Compared to $Cu_{50}Zr_{50}$, $Cu_{65}Zr_{35}$ not only has more icosahedra participating in ICOI, Fig. 4a, but also has a higher degree of ICOI as evaluated in terms of $N$, Fig. 4b. This makes $Cu_{65}Zr_{35}$ a more ordered structure with a higher atomic packing density and lower energy state.

## 5. Formation of ICOI network over extended range

Referring back to Fig. 3a, the spatial distribution of icosahedra is not uniform, but shows a large density variation. With a sufficiently high density of icosahedra participating

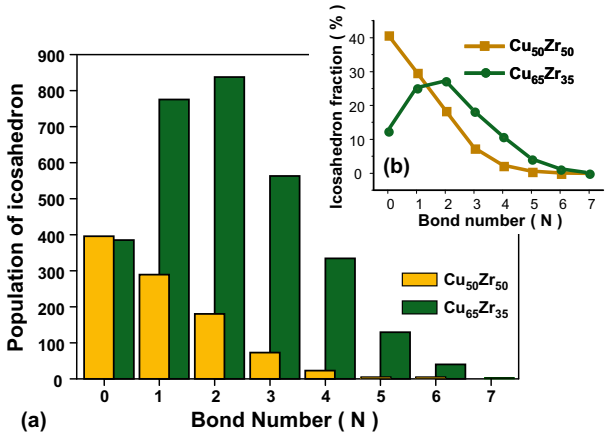


Fig. 4. Variations in (a) the population of various icosahedra and (b) heir fractions with different bond numbers in $Cu_{65}Zr_{35}$ and $Cu_{50}Zr_{50}$, showing that $Cu_{65}Zr_{35}$ has a higher degree of medium-range ordering as characterized by its higher population, and higher $N$, of icosahedra with ICOI.

in ICOI, they connect over an extended range, forming the basis for a networked structure. We therefore monitored the evolution of icosahedra in $Cu_{65}Zr_{35}$and $Cu_{50}Zr_{50}$during rapid cooling ($\sim 5 \times 10^{12}$ K $s^{-1}$) to examine how ICOI is developed.

Fig. 5a shows for the $Cu_{65}Zr_{35}$ alloy the variations in the fraction of icosahedra along with other populous SROs and low-population polyhedra, i.e., those with the coordination numbers (CN) that deviate substantially from 12. Also superimposed in the plot is the change in the potential energy (grey line) calculated at different cooling stages. Upon cooling, the fractional change of icosahedra was abrupt in the supercooled liquid regime, while the fractions of other SROs changed slightly. On the other hand, low-population polyhedra with lower symmetry decreased with cooling. During this evolution process, the smaller atoms (in this case, Cu), which are positioned on the coordination shell of an icosahedron, can also act as the center atoms of the neighboring icosahedra (see the inset of Fig. 2b), leading to various ICOIs with different $N$. Fig. 5b–d shows the representative snapshots of the icosahedral packing structures showing the evolution of ICOIs at different cooling stages. Considering that the potential energy of the system is lowered by forming ICOI via volume-sharing, this ICOI formation during cooling is natural and spontaneous.

It is noted from Fig. 5d that due to the lack of long-range periodicity of the icosahedra, the spatial distribution of the ICOIs (or icosahedra themselves) is not uniform, but rather exhibits a large density fluctuation. The volume-sharing ICOIs result in the formation of the string-like network. Fig. 6 is an example showing the largest ($1.2 \times 2.5 \times 2.2$ nm) ICOI network connected over an extended range. However, due to the "occasional" discontinuity with neighboring ICOIs, these ICOI patches do not result in a fully interconnected network structure that spans over the entire simulation cell (in this study, $7.9 \times 10.1 \times 6.4$ nm).

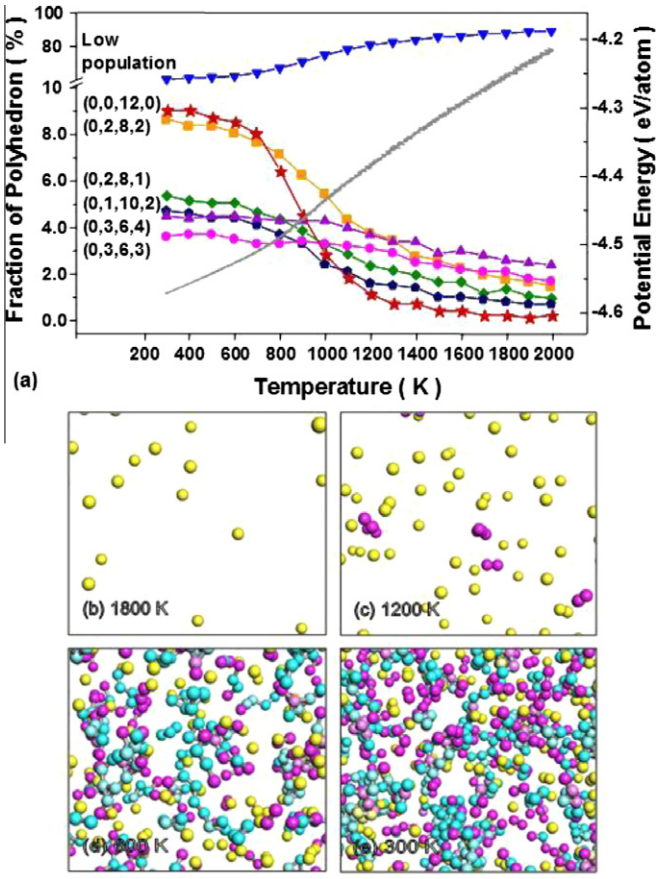


Fig. 5. (a) Evolution of various polyhedra with temperature during cooling, showing the abrupt change in the fraction of the icosahedra in the supercooled liquid region. Snapshots showing the icosahedral packing structures captured from the local regions of $1.2 \times 2.2 \times 4$ nm at temperatures of (b) 1800, (c) 1200, (d) 600 and (e) 300 K. In this figure, only the center atoms of the icosahedra are plotted as points in the simulation cell. Colors are added to indicate the formation of various types of ICOI characterized by the icosahedral bond numbers. (Yellow: $N = 0$, Purple: $N = 1$, Pale blue: $N = 2$, Pink: $N = 3$.) (For interpretation of the references to colour in this figure legend, the reader is referred to the web version of this article.)

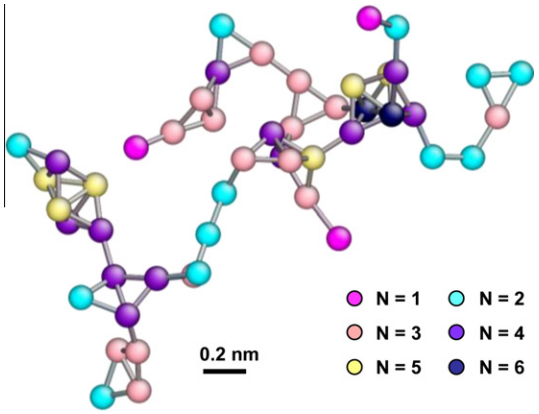


Fig. 6. Example of the extended ICOI network: a chain-like patch consisting of 55 icosahedra with different $N$. Only the center atoms of the icosahedra are plotted as points.

Table 2
Average atomic volume of the polyhedra with CN = 12 and the fractions that are interconnected to neighboring icosahedra by volume-sharing in $Cu_{65}Zr_{35}$. The average atomic volume here corresponds to the Voronoi volume calculated for the center atom (Cu) of each polyhedron.

| Polyhedron | $n$ | $n_V$ | $f(=n_V/n)$ (%) | $\overline{V}$ (A$^3$) |
|---|---|---|---|---|
| (0,0,12,0) | 3069 | – | – | 12.353 |
| (0,2,8,2) | 2935 | 1834 | 62.5 | 12.437 |
| (0,3,6,3) | 1422 | 759 | 53.4 | 12.795 |
| (0,4,4,4) | 452 | 154 | 34.1 | 12.610 |

*Note:* $n$ – total numbers of the polyhedron, $n_V$ – numbers of the polyhedron connected to (0,0,12,0) via volume sharing, $f$ – fractions of the polyhedron connected to (0,0,12,0) via volume sharing, $\overline{V}$ – average volume of the atom (Cu) centered at each polyhedron.

Having identified the extended-range patterns of ICOI, it is now of interest to examine how the spaces between the networked ICOI patches are filled with the remaining polyhedra. It is expected that SROs developed during cooling fill the 3D space in such a way that it lowers the potential energy of the system. Therefore, SROs with packing densities comparable to icosahedra tend to congregate next to the ICOIs, while SROs with comparatively loose atomic packing are further away from the ICOI, in order to reduce the abrupt density changes and the resulting strain misfit. Of the many relatively densely packed SROs, those with CN = 12, which we loosely call "icosahedron-like" polyhedra, are the plausible candidates capable of reducing the misfit strain by residing next to the ICOIs.

In order to determine the significant type of polyhedron that can reduce the misfit strain, we calculated both the atomic volume of the icosahedron-like polyhedra and their fractions of volume-sharing with neighboring icosahedra. According to the results in Table 2, of the several icosahedron-like polyhedra, (0,2,8,2) was not only statically dominant in terms of the population comprising the alloy, but also possesses the atomic volume close to that of the icosahedron. Therefore, we consider (0,2,8,2) to be the type of polyhedron capable of reducing the misfit strain when residing next to the ICOIs. Further, 36% and 63% of (0,2,8,2) in $Cu_{50}Zr_{50}$ and $Cu_{65}Zr_{35}$, respectively, were connected to the neighboring icosahedra via volume-sharing, as can be seen in Table 2. In fact, when considering every possible linking patterns (i.e., vertex-, edge-, face- and volume-sharing) of (0,2,8,2), the majority (83 and 99% for $Cu_{50}Zr_{50}$ and $Cu_{65}Zr_{35}$, respectively) of (0,2,8,2) were connected to neighboring icosahedra. As such, (0,2,8,2) can be regarded as the "glue polyhedron" that connects neighboring patches of ICOIs and helps extend/connect ICOI to longer range. The resulting networked ICOI structure is referred to as the "icosahedral network" in the following.

Fig. 7 is the snapshot showing the 3D packing structures of the icosahedra (each is denoted by a red solid ball) and (0,2,8,2) (denoted in green) comprising the model alloys. The regions indicated by the circles are magnified to show how (0,2,8,2) are connected to the patches of various ICOIs by sharing their volume. We first examined the qualitative effect of (0,2,8,2) on the enhancement of the connectivity of the ICOI in $Cu_{65}Zr_{35}$ and $Cu_{50}Zr_{50}$. In the case of $Cu_{50}Zr_{50}$, significant numbers of ICOIs were present as patches or islands, and thus fail to construct a well-interconnected network structure, even with the presence of (0,2,8,2), as shown in Fig. 7a. In contrast, most ICOIs in $Cu_{65}Zr_{35}$ are interconnected, although there exist occasional discontinuities. However, these breakage between the patches of ICOIs (and

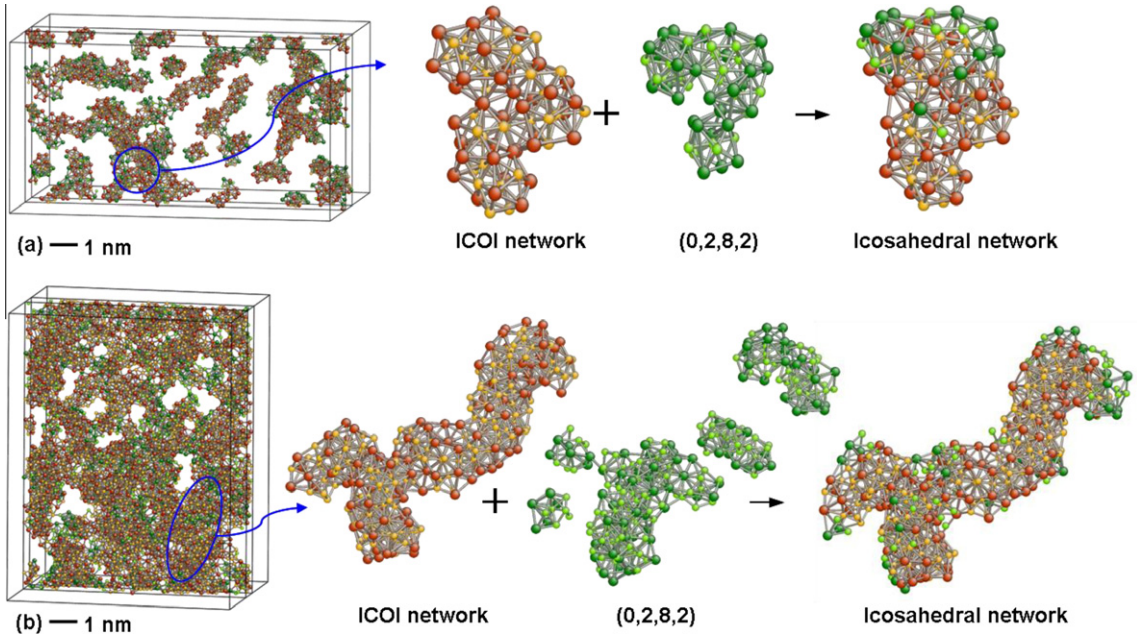


Fig. 7. Snapshots showing the spatial distribution of the ICOIs together with volume-sharing (0,2,8,2) that forms the icosahedral network structures in (a) $Cu_{50}Zr_{50}$ and (b) $Cu_{65}Zr_{35}$. Note that all (0,2,8,2) presented in the snapshots are connected to the neighboring ICOIs by sharing their volume, constructing the icosahedral network.

icosahedra) are connected by (0,2,8,2) via volume-sharing, which helps form an extensively interconnected icosahedral network, as shown in Fig. 7b.

We also examined the characteristics of the network structures to quantitatively assess: (1) how the glue polyhedron, (0,2,8,2), enhances the connectivity of the icosahedral network structures; and (2) whether the resultant structures are "weak" or "strong". First, the connectivity of the icosahedral network structures was evaluated by employing the connectivity parameter, $C$, which in this study is defined as

$$C_{ico} = \frac{n_I}{N_I} (\text{for icosahedra only}) \tag{1.1}$$

$$C_{network} = \frac{n_I + n_I' + n_D}{N_I + n_D} (\text{for icosaheral network}), \tag{1.2}$$

where $C_{ico}$ is the connectivity of the icosahedra by themselves, and $C_{network}$ the connectivity of the icosahedra along with (0,2,8,2). Here $N_I$ is the total number of icosahedra, and $n_I$ the numbers of the ICOIs themselves ($N \geqslant 1$ ICOIs), $n_I'$ the numbers of additional icosahedra connected by (0,2,8,2) via volume-sharing, and $n_D$ the numbers of (0,2,8,2) connected to neighboring icosahedra or (0,2,8,2) themselves via volume-sharing. Calculations showed that only 59% of icosahedra in $Cu_{50}Zr_{50}$ were connected to each other by sharing their volume, while 87% of icosahedra in $Cu_{65}Zr_{35}$ were the part of ICOIs. However, when incorporated with (0,2,8,2), this connectivity of icosahedra was increased to 90 and 98% for $Cu_{50}Zr_{50}$ and $Cu_{65}Zr_{35}$, respectively, as shown in Table 3. This supports the role of (0,2,8,2) as the glue polyhedron that can render better connectivity in forming the icosahedral network.

While the connectivity can be improved by the presence of (0,2,8,2), it does not establish whether the interconnected network structures are "weak" or "strong". This is because even with the same connectivity, the network structures can have a different spatial distribution of icosahedra and (0,2,8,2) in terms of their bond numbers and bond configurations (or geometry), resulting in different degree of clustering and thus rigidity. Recently, Wakeda and Shibutani [39] employed the clustering coefficient, $X$, to quantitatively assess the degree of local clustering of an icosahedral network structure. For the center atom of the $i$th icosahedron (or (0,2,8,2)) constituting the icosahedral network, $X_i$ is defined as [39,40]

$$X_i = \frac{2L_i}{N_i(N_i - 1)} \tag{2}$$

where $L_i$ is the number of ICOI with $N \geqslant 2$ having a triangular geometry and $N_i$ is the bond number of the $i$th icosahedron (or (0,2,8,2)) constructing an icosahedral network. Since the clustering coefficient not only considers the bond number, but also takes into account the geometric configuration of the icosahedral network structures, we consider the average value of $\overline{X}_{network}$ to be a suitable parameter that can reflect the rigidity of the network structure. As shown in Table 3, $\overline{X}_{network}$ was calculated to be 0.13 and 0.28 for $Cu_{50}Zr_{50}$ and $Cu_{65}Zr_{35}$, respectively, indicating that $Cu_{65}Zr_{35}$ has a more rigid icosahedral network structure than $Cu_{50}Zr_{50}$.

In view of the results discussed here, we can conclude that the characteristics of the icosahedral network rely on the initial packing state of the alloy, such that the more ordered alloy with a denser atomic packing ($Cu_{65}Zr_{35}$) has a much stronger tendency for the formation of the icosahedral network structure, while the alloy with looser atomic packing ($Cu_{50}Zr_{50}$) has a comparatively weak and loose one. However, looking at individual interconnected icosahedral network structures does not establish that there is a critical percolation over the entire sample in a way that would qualify the network as a "backbone" [11]. Therefore, the issue whether the amorphous alloy has a backbone remains an open question. Despite this ambiguity of the definition and actual presence of a backbone, real-world metallic glasses, due to their much slower cooling rate than that employed in simulations, should possess even higher fractions of SROs with CN = 12 than those described for the MD models. Therefore, ICOIs could/may eventually form a "percolating backbone" of the amorphous solid. While the high $C$ and $X$ discussed above for our icosahedra network is suggestive of a backbone structure, a quantitatively verifiable measurement of the connectivity, in terms of the backbone concept, needs systematic future work.

## 6. Stress-induced flow behavior

As discussed earlier, there are regions not covered by ICOIs and icosahedral networks. They correspond to comparatively loose packing, and thus can be fertile sites where local deformation nucleates. In other words, they can be fertile sites for potential shear transformation zones (STZs) under imposed stresses [6,41–43]. From this perspective, $Cu_{50}Zr_{50}$ should produce more potential STZs and can carry more strains prior to failure. In contrast, in the well-ordered $Cu_{65}Zr_{35}$ the icosahedral network is more

Table 3
Characteristics of the icosahedral network structures in $Cu_{50}Zr_{50}$ and $Cu_{65}Zr_{35}$ as quantified by their connectivity ($C$) and average clustering ($\overline{X}$) parameters.

| | Connectivity | | | | | | Rigidity | |
|---|---|---|---|---|---|---|---|---|
| | $N_I$ | $n_D$ | $n_I$ | $n_I'$ | $C_{ico}$ | $C_{network}$ | $\overline{N}_{network}$ | $\overline{X}_{network}$ |
| $Cu_{50}Zr_{50}$ | 968 | 652 | 572 | 238 | 0.59 | 0.90 | 0.67 | 0.13 |
| $Cu_{65}Zr_{35}$ | 3069 | 1834 | 2684 | 301 | 0.87 | 0.98 | 1.57 | 0.28 |

*Note:* $\overline{N}_{network}$ is the average bond number of the icosaheral network structure.

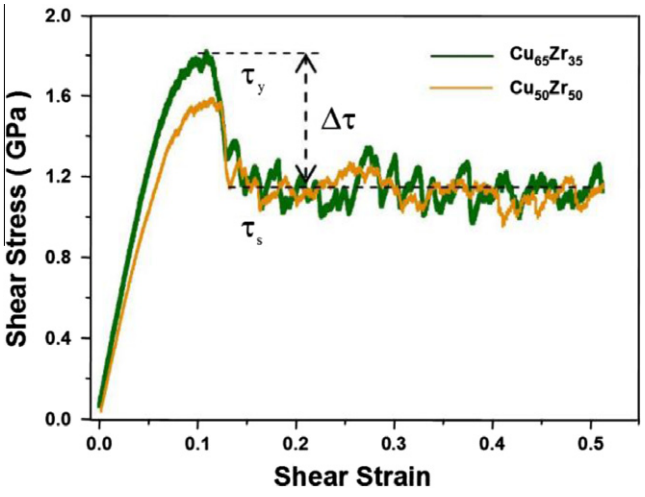


Fig. 8. Simulated stress–strain curves of the $Cu_{65}Zr_{35}$ and $Cu_{50}Zr_{50}$ amorphous solid calculated by the application of simple shear.

developed, compact and strong, which in turn can resist a higher load. However, due to the comparatively smaller flow regions within this alloy, it is unable to mediate large plastic strains. We believe that this difference in the atomic-scale structure of the alloys depicted via ICOI and icosahedral network would influence their mechanical responses associated with homogeneous and subsequent inhomogeneous deformation.

A number of experimental [27] and atomistic simulation [27,47] studies have suggested that the characteristics of homogeneous deformation are closely related to the dynamics of the inhomogeneous deformation (shear banding) and thus influence the global plasticity. In these previous studies, these deformation processes of metallic glasses were described by the structural evolution of SROs along with shear deformation [6,7,27]. Although the description based on SROs has been instructive for investigating the general features of the local deformation, the analyses limited to SRO are sometimes insufficient to explore the detailed principles underlying the homogeneous and inhomogeneous deformation [45]. In this section, we first monitor the mechanical response and associated structural evolution in terms of the fractional changes in SROs to elucidate the general features of local deformation. We then proceed to consider the shear transformations that involve ICOI and the icosahedral network.

Of the various bulk-forming Cu–Zr metallic glasses, $Cu_{65}Zr_{35}$ has the highest strength (~2.3 GPa) and lowest plasticity (0%), while $Cu_{50}Zr_{50}$ shows the lowest strength (~1.6 GPa) and highest plasticity (5%) [7,27,28]. The observed difference in the plasticity must be related to the shear banding behavior and correspond to the intrinsic atomic-scale structures of the alloys. Therefore, it is of interest to explore the flow characteristics of the amorphous solid inside a shear band and its associated disordering process. Fig. 8 shows the stress–strain curves of the model alloys calculated by applying simple shear strain. Considering that the dimensions of the samples used in this study are smaller than the typical thickness (10–20 nm) of a shear band, the mechanical responses of the model alloys in Fig. 8 can be regarded as the characteristic flow behaviors of the materials inside the shear band corresponding to each alloy. In both alloys, stress at first increases as deformation progresses. When it exceeds the critical strength ($\tau_y$), the alloys exhibit an abrupt decrease in strength. Beyond a shear strain of approximately 0.2, the stress tends to saturate to a steady-state value ($\tau_s$). The two stresses, $\tau_y$ and $\tau_s$, observed from the flow curves in Fig. 8, correspond to the characteristic strength reflecting the two different structural states of the amorphous solid [9]; $\tau_y$ is the stress required to initiate apparent plastic flow, i.e., a homogeneous shear of the entire simulation box (a small region inside a shear band) and thus corresponds to the global yield strength of the as-prepared amorphous solid. Once the amorphous solid begins to flow, structural disordering becomes significant [5,27,41,46–51], causing the material in the deformed regions to become softened and thereby achieving a steady-state flow. Therefore, $\tau_s$ can be regarded as the flow strength of the glass or the strength of a propagating shear band.

It is noted from Fig. 8 that $\tau_y$ is significantly higher in $Cu_{65}Zr_{35}$ than in $Cu_{50}Zr_{50}$, while $\tau_s$ is similar for the two compositions. As a result, the value of stress drop ($\Delta\tau = \tau_y - \tau_s$), i.e. softening, is greater for $Cu_{65}Zr_{35}$. Recent simulation studies and theoretical models have shown that the value of $\Delta\tau$ in Fig. 8 corresponds to a change in plastic response due to structural change in the glass, and that this structural softening determines the tendency towards strain localization and hence influences the plasticity of metallic glasses [6,44,49,52,53]. Since most mechanical properties are structure-dependent, the differences in the degree of softening of the model alloys must be related to the differences in the initial atomic-scale structures and their evolution during the homogeneous deformation.

## 7. Nucleation of local shear transformation and the stability of ICOI

It is known that the "homogeneous" plastic deformation preferentially occurs at the local regions with loose atomic packing even under stresses that are well below the global yield [5,7–10,27,47,48,54,55]. This deformation causes structural disordering, i.e., the creation of new, loosely packed SROs appearing at the expense of densely packed polyhedra, such as icosahedra ("partial" dissolution of icosahedra such that the entire box can globally flow at the imposed strain rate) [9,55–57]. We have examined in more detail the structural stability of the icosahedra and various other SROs. We do so by subtracting uniform cell deformation corresponding to global shear strain and calculating the non-affine atomic displacement as evaluated by the non-affine strain residue of the center atoms of the corresponding SROs. The procedures are identical to those published in Refs. [9,58].

Fig. 9a shows the distribution of the non-affine displacement of the constituent atoms in $Cu_{65}Zr_{35}$ subjected to a shear strain ($\gamma$) of 0.1. The constituent atoms of the model alloy were divided into five groups based on the magnitude of their non-affine displacement, with each group corresponding to 20% of the total number of atoms, in order to examine the origin of the differences in the atomic mobility. Then the atoms of each group, each as the center atom of certain SROs, were analyzed in order to identify the atoms' local environment, i.e., the type of polyhedron the atom is in, and are labeled using different colors in Fig. 9b. Some important findings emerge from these analyses. First, the fraction of the icosahedra was the largest (~13%) in the group with the smallest displacement, but the lowest (~5%) in the group showing the largest displacement [9]. These results indirectly confirmed the previous results that shear transformation is favored at regions with less order [5,9,10] and relatively loose atomic packing [6,7,27]. The fact that atoms were displaced from their initial position does not necessarily induce the disruption of SROs and icosahedra. However, the present analyses lend support to the idea that an icosahedron would be structurally more stable and thus exhibit higher resistance to shear deformation.

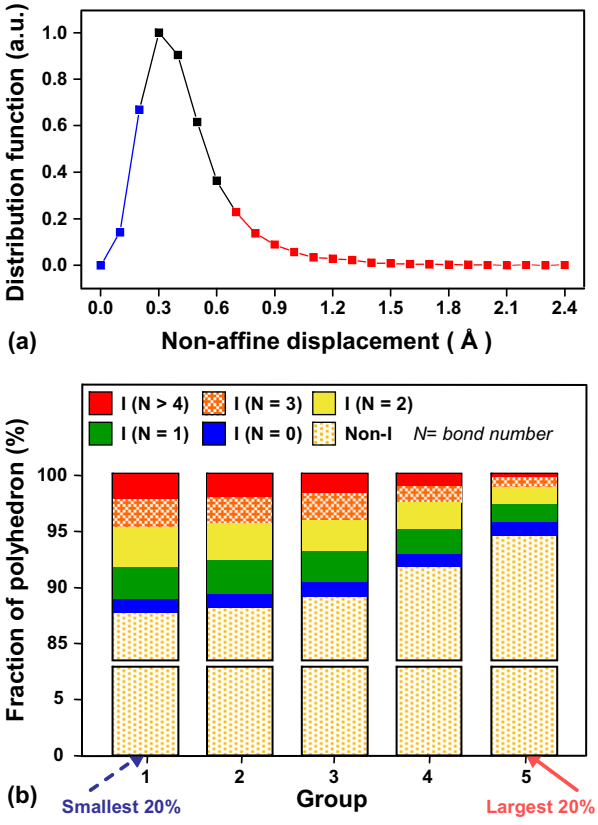


Fig. 9. (a) Distribution of the non-affine displacement of the constituent atoms of $Cu_{65}Zr_{35}$ as a result of the homogeneous deformation ($\gamma = 0.1$). (b) All atoms were sorted by their atomic displacement from low to high, and divided into five groups, with each group corresponding to 20% of the total number of atoms. In each group, the atoms were categorized by the atoms' occupation as the center atom of certain SROs.

The structural stability of the icosahedra was also quantitatively evaluated by measuring the fractions of the icosahedra that were destroyed and transformed during the homogeneous deformation ($\gamma = 0.1$), as a function of $N$. Comparing the structures before and after the deformation, the icosahedra that bond to fewer neighboring icosahedra (smaller $N$ for ICOI) were more prone to disruption, whereas the icosahedra with high $N$ displayed comparatively less structural changes, as shown in Fig. 10a. Since the structural stability is related to the potential energy, the average potential energy of the center atom (Cu) of each icosahedron was calculated with respect to its bond number$N$as shown in Fig. 10b. The potential energy of the center atoms of the icosahedra in $Cu_{65}Zr_{35}$ decreased with increasing $N$. (A similar tendency was also observed in $Cu_{50}Zr_{50}$.) This indicates that the icosahedron becomes structurally and energetically more stable by joining ICOI with neighboring icosahedra. This is the underlying physical origin as to why the mobility of the atoms becomes lower as they form ICOI. The lowered atomic mobility (and local structural changes) in turn hinders the formation of new STZs required for plastic flow, thus restricting the spreading of plastic strain. Therefore, during deformation of $Cu_{65}Zr_{35}$, strains would be more likely to be localized in a smaller number of already-deformed regions (such as shear bands) rather than spreading out to other less-deformed regions that still have a high degree of ICOI.

## 8. Collapse of the icosahedral network and shear localization

The discussion in the previous section indicates an important feature that a higher degree of ICOI corresponds to fewer numbers of STZs, suggesting a possible correlation between the ordered structures in the medium-to-

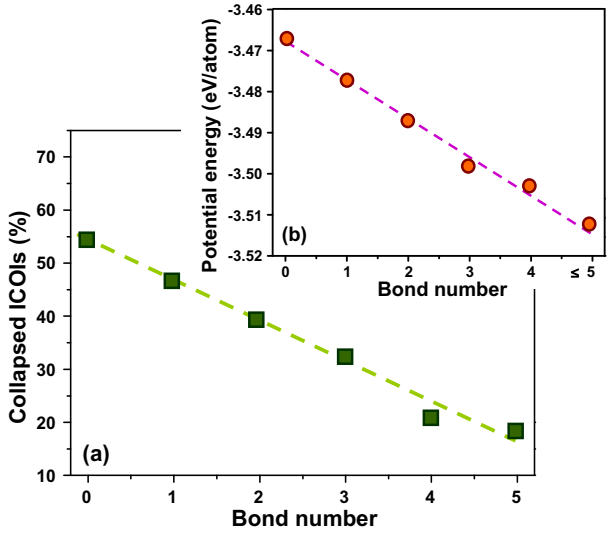


Fig. 10. (a) Fractional change of the ICOIs, which were destroyed through simple shear ($\gamma = 0.1$), as a function of the bond number. (b) Average potential energy of the center atoms (Cu) of the icosahedra (with the common composition of $Cu_6Zr_7$) as a function of the bond number of the ICOI.

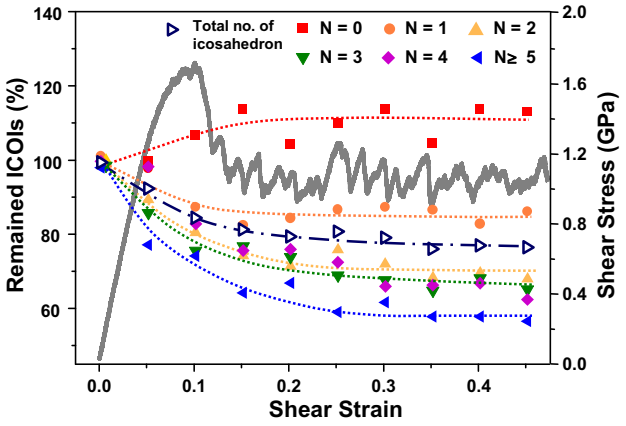


Fig. 11. Fractional changes of the various ICOIs in $Cu_{65}Zr_{35}$ as a function of the shear strain. The results are superimposed with the changes in the stress corresponding to the applied strain.

extended range and the plasticity of metallic glasses. This qualitative analysis provides additional valuable insight into the underlying physics as to why more ordered alloys exhibit more intense shear localization associated with the inhomogeneous deformation, i.e., lower plasticity.

The changes in the fraction of ICOIs with different $N$ were monitored with respect to the shear strain to further understand the structural origin of the shear instability that occurs beyond the global yield. During deformation, both the disruption and the creation of the icosahedra take place simultaneously [45], although their rates are different depending on the testing temperature and strain imposed to the sample. As such, in this study, both the disrupted and new-born icosahedra were counted in the analyses to correlate with the flow stress. Shown in Fig. 11 are the fractional changes of the ICOIs plotted with respect to different $N$ and shear strain. Also superimposed in the plot is the stress–strain curve of $Cu_{65}Zr_{35}$. As the deformation proceeded, the ICOIs ($N \geqslant 1$) suffered from disruption, while the population of the non-interpenetrating icosahera increased. The disruption of the ICOIs was more prominent for ICOIs with higher$N$. This is because, to sustain the global flow at the imposed strain rate, new STZs have to be additionally supplied, and the icosahedral network structure has to give up to allow strain compatibility and sufficiently low viscosity. However, when counting the total population of icosahedra (see the "1" symbol in the graph), this structural state was almost saturated at strains beyond $\gamma > 0.2$, achieving a steady-state flow [59].

Fig. 12 is the graphical illustration of Fig. 11, showing a detailed sequence of the collapse of the icosahedral network structure with increasing strain. The points in Fig. 12a correspond to all atoms that comprise the ICOI in the icosahedral network structure of $Cu_{65}Zr_{35}$ and are labeled in different colors to distinguish Cu (yellow) from Zr (blue). In order to better visualize the structural changes

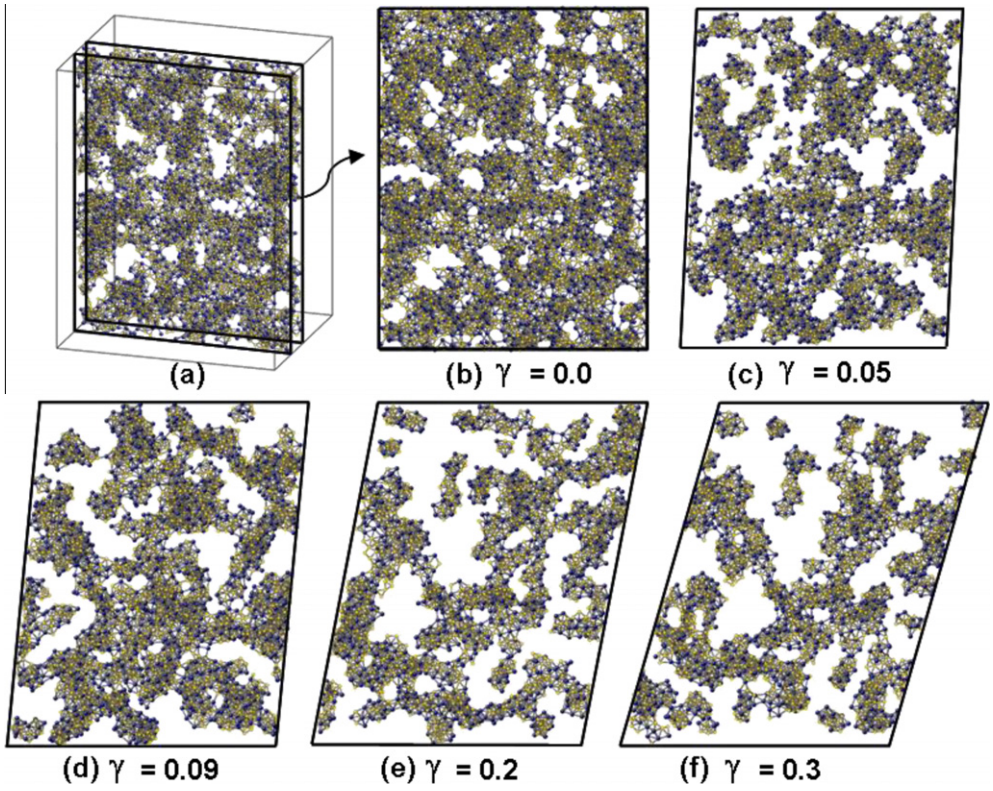


Fig. 12. 3D configuration of the ICOI at various deformation stages, showing the collapse of the icosahedral network structure through the disruption of ICOI. Only the ICOI within the thickness of ~1 nm in (a) were shown in order to better illustrate the structural evolution sequence. (b) $\gamma = 0.0$, (c) $\gamma = 0.05$, (d) $\gamma = 0.09$, (e) $\gamma = 0.2$, (f) $\gamma = 0.3$.

of ICOI associated with deformation; only the ICOI within a slab with the thickness of ~1 nm were shown. At a very early stage of the homogeneous deformation ($\gamma < 0.05$), the ICOIs with smaller $N$ (equivalently, those surrounded by loosely packed SROs) tend to break down. Upon further loading exceeding the global yield ($\gamma > 0.1$), the ICOI with larger $N$ suffered from preferential disruption, which broke the icosahedral network structure. Beyond $\gamma > 0.2$, the apparent structural disorder reached a steady state. Therefore, the disruption of the structurally stable icosahedral network was necessary for the onset of the global plastic flow. During this disordering process, the ICOI with large $N$ were converted to the ones with smaller $N$, which not only acts as the source of new STZs but also results in structural softening.

## 9. Conclusion

In the present study, the glassy structure and its role on the propensity for plastic relaxation of the metallic glasses have been assessed in terms of the fractions of ICOIs and their "bond numbers" ($N$, the degree of volume-sharing connection to form ICOI). This treatment considering the medium-range structures and their network connections over extended range provides important details extending earlier modeling on the effect of SROs and the percolation of SROs.

$Cu_{65}Zr_{35}$ with dense atomic packing [55,57] is associated with large fractions of ICOIs with high $N$, such that the icosahedra will be more extensively connected to one another in an interpenetrating fashion, constituting a compact icosahedral network over an extended range. The icosahedral network structure is resistant to stress-induced shear transformations under applied load, and needs to be broken down to soften the glass for homogeneous flow. Therefore, a well-ordered $Cu_{65}Zr_{35}$, which is characterized by the extensive network structure and comparatively smaller number of flow regions, is less likely to accommodate large strains through spread-out shear transformations. As a result, the degree of softening associated with the disruption of ICOI and network in $Cu_{65}Zr_{35}$ would be more pronounced, and likely to result in more obvious strain localization and lower plasticity.

## Acknowledgements

JC acknowledges the support of the National Research Foundation of Korea under Award of 2009-0081023. EM is supported at JHU by US-NSF-DMR-0904188. A major part of the present computation was carried out using the Grand Cluster Supercomputer at KIST.

## References

[1] Ramsey FP. Econ J 1928;38:543.
[2] Miracle DB. Acta Mater 2006;54:4317.
[3] Sheng HW, Cheng YQ, Lee PL, Shastri SD, Ma E. Acta Mater 2008;56:6264.
[4] Yang L, Jiang JZ, Liu T, Hu TD, Uruga T. Appl Phys Lett 2005;87:061918.
[5] Shi Y, Falk ML. Phys Rev B 2006;73:214201.
[6] Wakeda M, Shibutani Y, Ogata S, Park JY. Intermetallics 2007;15:139.
[7] Lee JC, Park KW, Kim KH, Fleury E, Lee BJ, Wakeda M, et al. J Mater Res 2007;22:3087.
[8] Park KW, Jang JI, Wakeda M, Shibutani Y, Lee JC. Scripta Mater 2007;57:805.
[9] Cheng YQ, Cao AJ, Sheng HW, Ma E. Acta Mater 2008;56:5263.
[10] Shi Y, Falk ML. Phys Rev Lett 2005;95:095502.
[11] Shi Y, Falk ML. Scripta Mater 2006;54:381.
[12] Voyles PM, Muller EA. Ultramicroscopy 2002;93:127.
[13] Treacy MMJ, Gibson JM. Acta Cryst A 1996;52:212.
[14] Voyles PM, Gerbi JE, Treacy MMJ, Gibson JM, Abelson JR. Phys Rev Lett 2001;86:5514.
[15] Miracle DB. Nature Mater 2004;3:697.
[16] Sheng HW, Luo WK, Alamgir FM, Bai JM, Ma E. Nature 2006;439:419.
[17] Wang XD, Yin S, Cao QP, Jiang JZ, Franz H, Jin ZH. Appl Phys Lett 2008;92:011902.
[18] Wang SY, Wang CZ, Li MZ, Huang L, Ott RT, Kramer MJ, et al. Phys Rev B 2008;78:184204.
[19] Hufnagel TC. Phys Rev B 2003;67:014203.
[20] Fan C, Wilson TW, Dmowski W, Choo H, Richardson JW, Maxey ER, et al. Intermetallics 2006;14:888.
[21] Hui X, Gao R, Chena GL, Shang SL, Wangb Y, Liub ZK. Phys Lett A 2008;372:3078.
[22] Hui X, Fang HZ, Chen GL, Shang SL, Wang Y, Qin JY, et al. Acta Mater 2009;57:376.
[23] http://sites.google.com/a/gmu.edu/eam-potential-database/.
[24] Hoover. Phys Rev A 1985;31:1695.
[25] Hoover. Phys Rev A 1986;34:2499.
[26] Richards FM. J Mol Biol 1974;82:1.
[27] Park KW, Lee CM, Wakeda M, Shibutani Y, Falk ML, Lee JC. Acta Mater 2008;56:5440.
[28] Lee SW, Huh MY, Fleury E, Lee JC. Acta Mater 2006;54:349.
[29] Cheng YQ, Ma E, Sheng HW. Phys Rev Lett 2009;102:245501 (see EPAPS Document No. E-PRLTAO-103-011927 for supplemental materials at <http://www.aip.org/pubservs/epaps.html>).
[30] Chen HS, Waseda Y. Phsy Stat Sol(a) 1979;51:593.
[31] Bionducci M, Licheri G, Navarra G, Bouchet-Fabre b. J Phys Sci 1996;51:71.
[32] Matterna N, Schöpsb A, Kühna U, Ackera J, Khvostikovaa O, Eckerta J. J Non-Cryst Solids 2008;354:1054.
[33] Kim YM, Lee BJ. J Mater Res 2009;23:1095.
[34] Bubanov YA, Schvetsov VR, Siderenko AF. Phys B 1995;95:208.
[35] Paduraru A, Kenoufi A, Nicholas P, Bailey A, Schiøtz j. Adv Eng Mater 2007;9:505.
[36] Sadoc A, Clavayraac Y, Quivy A, Harmelin M, Flank AM. J Non-Cryst Solids 1984;65:109.
[37] Duan G, Xu D, Zhang Q, Cagin T, Johnson WL, Goddard WA. Phys Rev B 2005;71:224208.
[38] Shimono M, Onodera H. Mater Sci Forum 2007;539:2031.
[39] Wakeda M, Shibutani Y. Acta Mater 2010;58:3963.
[40] Watts DJ, Strogatz SH. Nature 1988;393:440.
[41] Falk ML, Langer JS. Phys Rev E 1998;57:7192.
[42] Falk ML. Phys Rev B 1999;60:7062.
[43] Schuh CA, Lnd AC, Nieh TG. Acta Mater 2004;52:5879.
[44] Shi YF, Katz MB, Li H, Falk ML. Phys Rev Lett 2007;98:185505.
[45] Lee CM, Park KW, Lee BJ, Shibutani Y, Lee JC. Scripta Mater 2009;61:911.
[46] Argon AS. Acta Metall 1979;27:47.
[47] Lee SC, Lee CM, Lee JC, Kim HJ, Shibutani Y, Fleury E, et al. Appl Phys Lett 2008;92:151906.
[48] Cao AJ, Cheng YQ, Ma E. Acta Mater 2009;57:5146.
[49] Lee SC, Lee CM, Yang JW, Lee JC. Scripta Mater 2007;58:591.
[50] Tomida T, Egami T. Phys Rev B 1993;48:3048.

[51] Ogata S, Shimizu F, Li J, Wakeda M, Shibutani Y. Intermetallics 2006;14:1033.
[52] Manning ML, Langer JS, Carlson JM. Phys Rev E 2007;76:056106.
[53] Manning ML, Daub EG, Langer JS, Carlson JM. Phys Rev E 2009;79:016110.
[54] Lee SJ, Yoo BG, Jang JI, Lee JC. Met Mater Int 2008;14:9.
[55] Park KW, Wakeda M, Shibutani Y, Fleury E, Lee JC. Met Mater Int 2008;14:159.
[56] Lee CM, Park KW, Lee JC. J Kor Inst Met Mater 2008;46:707.
[57] Park KW, Lee CM, Lee JC. J Kor Inst Met Mater 2009;47:773.
[58] Wakeda M, Shibutani Y, Ogata S, Park J. Intermetallics 2007:15 139.
[59] Albano F, Falk ML. J Chem Phys 2005;122:154508.
[60] Sinclair F. Phil Mag A 1984;50:45.